PAPER

Simulation of MHD instabilities with fluid runaway electron model in M3D-C^1

To cite this article: C. Zhao *et al* 2021 *Nucl. Fusion* **60** 126017

IOP Publishing | International Atomic Energy Agency Nuclear Fusion

Nucl. Fusion **60** (2020) 126017 (7pp) https://doi.org/10.1088/1741-4326/ab96f4

Simulation of MHD instabilities with fluid runaway electron model in M3D-C^1

C. Zhao, C. Liu, S. C. Jardin and N. M. Ferraro

Princeton Plasma Physics Laboratory, P.O. Box 451, Princeton, New Jersey 08543-0451, United States of America

E-mail: czhao@pppl.gov

Received 9 April 2020, revised 23 May 2020
Accepted for publication 27 May 2020
Published 26 October 2020

Abstract

Runaway electrons may be generated in a tokamak during the start up, during normal operation and during a plasma disruption. During a disruption, runaway electrons can be accelerated to high energies, potentially damaging the first wall. To predict the consequences of runaway generation during a disruption, it is necessary to consider resonant interactions of runaways with the bulk plasma. Here we consider the interactions of runaways on low mode number tearing modes. We have developed a fluid runaway electron model for the 3D MHD code M3D-C^1 (Jardin *et al* 2012 *J. Comput. Sci. Discovery* **6** 014002). To benchmark, we have reproduced the MHD linear tearing mode results (with runaway electrons) in a circular cylinder presented in previous analytic studies (Helander *et al* 2007 *Phys. Plasmas* **14** 104142) and have extended them here with a numerical eigenvalue calculation. We find that the low mode number tearing mode has a rotation caused by the MHD - runaways interaction and the perturbed toroidal current scale length is much smaller with runaways than without and decreases as the runaway speed increases.

Keywords: runaway electron, MHD instability, M3D-C1 code

(Some figures may appear in colour only in the online journal)

1. Introduction

In the first phase of a typical tokamak disruption, confinement is lost and a "thermal quench" occurs, drastically decreasing the temperature of the discharge and thereby increasing its resistivity, $\eta \sim T_e^{-3/2}$. The increased resistivity produces a large electric field parallel to the magnetic field, $\mathbf{E}_{||} = \eta \mathbf{J}_{||}$ where $\mathbf{J}_{||}$ is the electrical current density parallel to the magnetic field. This, in turn, causes the "current quench" in which the tokamak plasma current decays in this highly resistive plasma. During the current quench, the parallel electric field can often exceed the critical electric field for runaway generation [1–3] causing a runaway electron population to form. The electrical current from these runaway electrons can continue to increase as the current from the bulk electrons decreases, until the entire discharge current is being carried by the runaways. This paper is concerned with calculating the macroscopic stability of these runaway discharges.

Section 2 describes the fluid runaway electron model that has been incorporated into the initial-value M3D-C^1 code [4]. Section 3 describes a method we have developed to solve for linear MHD stability as an eigenvalue problem using the reduced MHD equations but including the fluid runaway terms. In section 4 we present solutions of the linearized MHD equations, including runaways, described in section 2 and compare the results with those of the eigenvalue approach for both a (1,1) and (2,1) resistive instability. Section 5 presents a summary and conclusions.

2. Fluid runaway electron model in M3D-C^1

The M3D-C^1 code is an implicit extended-magnetohydrodynamic (MHD) code that utilizes high-order C^1 continuous finite elements in three dimensions. It has options for reduced MHD or full MHD, linear or non-linear, cylindrical or toroidal geometry. It includes options for impurity transport and radiation [5] and the interaction of the tokamak plasma with a resistive wall [6]. The code uses an unstructured mesh in the

(R,Z) plane (cylindrical or Cartesian coordinates). For nonlinear 3D calculations the mesh is extruded in a structured way in the third dimension to form triangular prism elements. The unstructured triangular mesh is constructed using a user-defined "size field" and can thus be made to have small triangles and hence high resolution around certain rational surfaces or other locations where large gradients are expected to develop [7].

We have implemented a fluid runaway electron model in M3D-C^1 which is similar to that used in previous studies [8–10], although the curvature drift term in [8] is not included. The total runaway current density J_{RE} is represented as

$$\mathbf{J}_{RE} = -n_{RE}e(c\frac{\mathbf{B}}{B} + \frac{\mathbf{E}\times\mathbf{B}}{B^2}). \tag{1}$$

Here E and B are the electric and magnetic fields. The runaway electron number density obeys the continuity equation

$$\frac{\partial n_{RE}}{\partial t} - e^{-1}\nabla\cdot\mathbf{J}_{RE} = S_{RE}. \tag{2}$$

Here S_{RE} is the runaway source rate, including Dreicer [1] and avalanche [2] mechanisms.

As introduced in section 1, the runaway electron current can interact with the bulk plasma. We apply the fluid model runaway current in the bulk plasma momentum time advance as

$$\rho\frac{d\mathbf{V}}{dt} = (\mathbf{J}-\mathbf{J}_{RE})\times\mathbf{B} - \nabla p + en_{RE}\mathbf{E}. \tag{3}$$

Here the last term is present when deriving a bulk fluid momentum equation when runaways are present so that $n_{RE}+n_e = n_i$ and by ignoring the inertia of the runaways [8]. Inserting equation (1) into equation (3), the magnetic force caused by the $E\times B$ drift of the runaways cancels the perpendicular electric force of the runaways and we have

$$\rho\frac{d\mathbf{V}}{dt} = \mathbf{J}\times\mathbf{B} - \nabla p + en_{RE}\mathbf{E}\cdot\hat{\mathbf{b}}\hat{\mathbf{b}}. \tag{4}$$

Here $\hat{\mathbf{b}} = \mathbf{B}/B$ is the unit vector along the field line. To be consistent with the Helander model [12] which we used in section 3, we did not include the last term in equation (4). The resistivity only affects the current carried by the bulk electrons, so that the generalized Ohm's law becomes:

$$\mathbf{E} + \mathbf{V}\times\mathbf{B} = \eta(\mathbf{J}-\mathbf{J}_{RE}) \tag{5}$$

We presently time advance the magnetic field using the split-implicit method described in [4] using a fixed runaway density and then time advance the runaway density by solving equation (1) and (2) implicitly for n_{RE} using the θ-implicit method [11], but using fixed magnetic and electric fields. The momentum is conserved in this fluid runaway electron model in the limit that the momentum and drag of the runaway electrons is negligible. In the linearized equations solved here, the bulk fluid density is not advanced in time.

3. Eigenvalue solution from reduced MHD equations with runaway electrons

We have developed a numerical procedure to solve the set of reduced MHD equations with runaways [12] as a generalized eigenvalue problem. Consider the linearized equations:

$$\omega\psi - k_{||}\phi = i\eta\left(\nabla_\perp^2\psi + j\right), \tag{6}$$

$$\omega\nabla_\perp^2\phi - k_{||}\nabla_\perp^2\psi = \frac{mj_0'}{r}\psi, \tag{7}$$

$$\left(k_{||}+\omega v_A/c\right)j = \frac{mj_{RE0}'}{r}\left(\psi + v_A\phi/c\right), \tag{8}$$

Here (ψ,ϕ,j) are the normalized linearized magnetic vector potential, electric potential and runaway current density perturbation. They are taken to vary in space in time as (cylindrical coordinates) $\psi(r,\theta,z,t) = \psi(r)e^{i(nz-m\theta-\omega t)}$, $\nabla_\perp^2 = d/rdr(rd/dr) - m^2/r^2$, ( ) means d(...)/dr, j_0 is the total equilibrium current, j_{RE0} is the equilibrium runaway current, $k_{||} = n - m/q(r)$, v_A is the Alfven velocity based on the toroidal magnetic field and c is the speed of the runaway electrons. Note that $\omega = \omega_r + i\gamma$ is a complex number containing the real frequency and the growth rate of the mode. Equations (6)–(8) can be written in matrix form

$$\omega\begin{bmatrix} I & 0 & 0\\ 0 & \nabla_\perp^2 & 0\\ 0 & 0 & v_A/c\end{bmatrix}\begin{bmatrix}\psi\\ \phi\\ j\end{bmatrix} = \begin{bmatrix} i\eta\nabla_\perp^2 & k_{||} & i\eta\\ k_{||}\nabla_\perp^2 + mj_0'/r & 0 & 0\\ mj_{RE0}'/r & mj_{RE0}'v_A/rc & -k_{||}\end{bmatrix}\begin{bmatrix}\psi\\ \phi\\ j\end{bmatrix}. \tag{9}$$

We next apply the finite difference method to equation (9). The continuous functions $\psi(r),\phi(r),j(r)$ are replaced by their values at $N+1$ equally spaced discrete points: $r_i = i\delta r$ for $i = 0,...,N$ where $\delta r = a/N$. Using standard centered second-order finite differences for the derivative operator, equation (9) becomes a 3 N× 3 N discrete generalized eigenvalue matrix equation that can be solved by standard techniques. Boundary conditions are: $\psi(0) = \psi(a) = 0, \phi(0) = \phi(a) = 0, j(0) = j(a) = 0$.. The beta was 1.10^{-7} and the density was uniform since we are trying to model a post-thermal quench plasma where the beta is near zero and all the current is being carried by the runaways. Note that we do not include the runaway source terms since we are focusing on the runaway-MHD interaction and the runaway generation rate is much smaller than the MHD instabilities growth rate.

3.1. $m = 1$, $n = 1$ resistive kink mode

Consider a cylindrical equilibrium with $q(r) = 0.85 + 3.4(r/a)^2$ as shown in figure 1 and with inverse aspect ratio

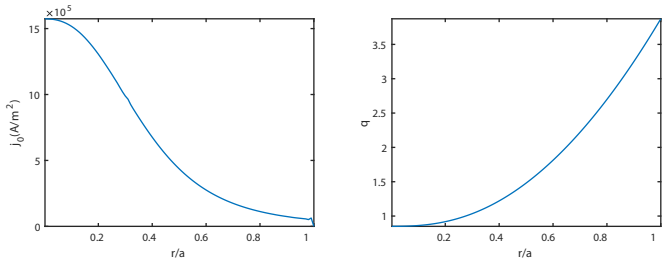

Figure 1. (*a*) Current profile and the (*b*) safety factor profile for (1,1) resistive kink mode with run away electron simulation.

$\varepsilon = 0.1$. With the full equilibrium current being carried by the runaway electrons, i.e. $j_0 = j_{RE0}$ in equation (9), we solve for the stability of the m = 1, n = 1 mode. The unstable eigenfunction for the magnetic flux and runaway electron current density are shown in figures 2(*a*) and (*b*) for a case with $\eta/\mu_0 v_A \epsilon a = 2\times10^{-5}, c/v_A = 200, N = 5000$ intervals. For comparison, we also show in figure 2 the eigenfunction of a conventional resistive kink for the same equilibrium but with $j_{RE0} = 0$.

It is seen that the mode structure of the real part of magnetic flux ψ for the runaway discharge is the same as that for the conventional (1,1) resistive kink mode structure [13] but it also has a non-zero imaginary part which the conventional discharge does not. It is seen in figures 2(*b*) and (*c*) that the runaway current is much more highly peaked around the $q = 1$ surface at $r = 0.275a$, with the scale length about $10^{-3}a$, than is the toroidal current of the conventional (1,1) resistive kink mode (scale length about $0.1a$) and it also has a highly peaked imaginary part while the conventional (1,1) mode does not, which confirms previous studies [9].

The real frequency and growth rate for this case are 0.011 v_A/a and 0.035 2 v_A/a. For the conventional (1,1) resistive kink mode, the growth rate is 0.028 3 v_A/a and the real frequency is zero [13, 14]. The fact that we are finding a non-zero real frequency when runaways are included implies that the runaway electron current can interact with the (1,1) resistive kink mode to give the mode a rotation. In our calculation, the non-uniformity of the equilibrium runaway current jre_0 is the main factor which causes the mode to have an imaginary part. If we set $jre_0' = 0$, using a uniform equilibrium runaway current profile, the eigenvalue changes from (0.011, 0.035 2) to (0.000,0.035 2) and the imaginary part of the magnetic flux and current disappears. The reason for this can be seen from equation (8). If the equilibrium runaway current gradient vanishes, the runaway current perturbation does not affect the electric and magnetic field of bulk plasma, which implies that without runaway-MHD interactions, the rotation will not occur. This indicates that the rotation driven by the runaway current is mainly due to the gradient of the runaway electron current.

The speed of the runaway electrons, that we have been denoting by c, also affects the (1,1) resistive kink mode. As shown in figure 3(*a*), when $c < 10v_A$, both the mode growth rate and real frequency increase almost linearly with c/v_A until $c/v_A = 10$, at which point they become almost independent of

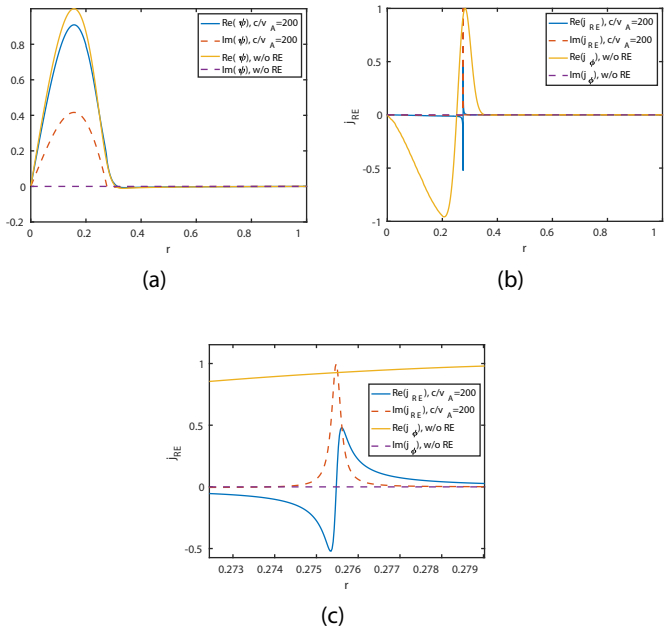

Figure 2. (*a*) Magnetic flux structure, (*b*) runaway/toroidal current structure and (*c*) close up of runaway current structure near the singular surface of the (1,1) resistive kink mode with and without runaway electrons.

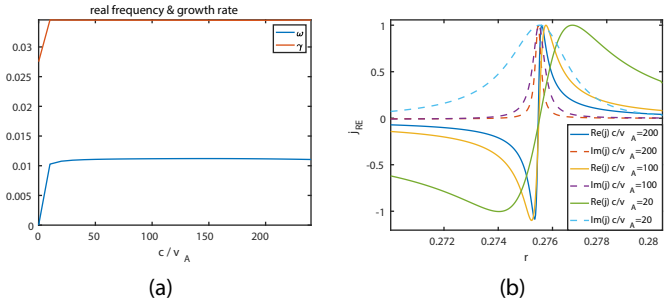

Figure 3. (*a*) eigenvalues and (*b*) current structures of (1,1) resistive mode with runaway electrons with different runaway speed.

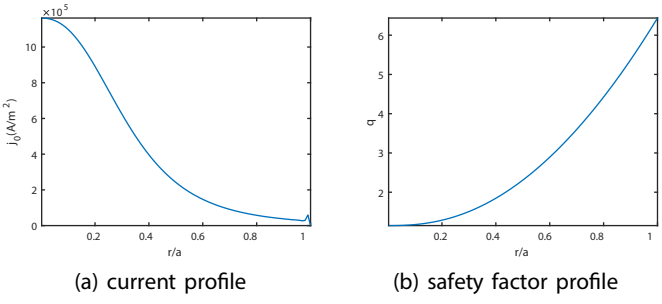

Figure 4. (*a*) Current profile and the (*b*) safety factor profile for (2,1) tearing mode with run away electron simulation.

it. The scale length of the radial structure of the perturbed current density does, however, depend on the magnitude of c/v_A as shown in figure 3(*b*). The scale length becomes smaller at higher runaway speeds [12] even as the growth rate and real frequencies remain fixed.

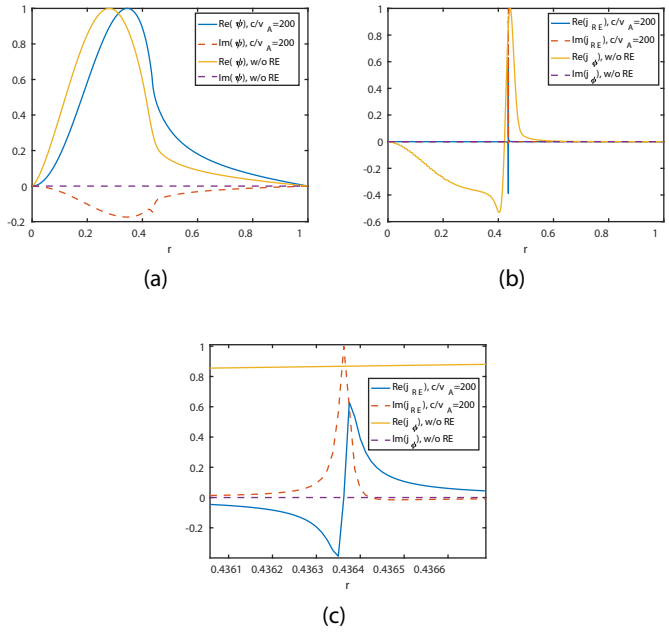

Figure 5. (*a*) Magnetic flux structure, (*b*) runaway/toroidal current structure and (*c*) close up of the runaway current structure near singular surface of the (2,1) tearing mode with runaway electrons.

3.2. $m = 2$, $n = 1$ tearing mode

We have also calculated the eigenmodes and eigenfunction of a m = 2, n = 1 mode in the equilibrium shown in figure 4 with $q(r) = 1.15 + 5.75(r/a)^2$ for a case with $\eta/\mu_0 v_A \epsilon a = 2 \times 10^{-5}, c/v_A = 200$, inverse aspect ratio $\varepsilon = 0.1$, $N = 8000$ intervals. Figure 5(*a*) shows that the magnetic flux of the (2,1) tearing mode with runaways also has an imaginary part and the real part is shifted relative to the non-runaway structure. The (2,1) tearing mode is thus more perturbed by the runaway current than is the (1,1) resistive kink mode. Figures 5(*b*) and (*c*) shows that the eigenfunctions corresponding to the current density when runaways are present are much more peaked at the $q = 2$ surface than for the conventional (2,1) tearing mode. It also has an imaginary part which the conventional tearing mode does not.

The eigenvalue for the configuration with runaways was found to be $\gamma = 0.00627 v_A/a, \omega_r = -0.0088 v_A/a$, compared to $\gamma = 0.00613 v_A/a, \omega_r = 0$ when runaways are absent. We have also verified that, as for the (1,1) mode, forcing the current density gradient to vanish reduced the imaginary eigenstructure and real frequency to 0. The effect of the runaway electron velocity on the current eigenmode is also similar to that shown in figure 3 for the (1,1) mode, but the scale length of the (2,1) tearing mode is about $10^{-4}a$, which is much smaller than that for the (1,1) resisitive kink mode with the same runaway speed as shown in figure 6

4. M3D-C^1 linear simulations with fluid model runaway electrons

Here we compute the stability of the same class of equilibria considered in section 3, but using the time-dependent M3D-C^1 code. To be consistent, we have run the code in the cylindrical, reduced MHD and linear modes.

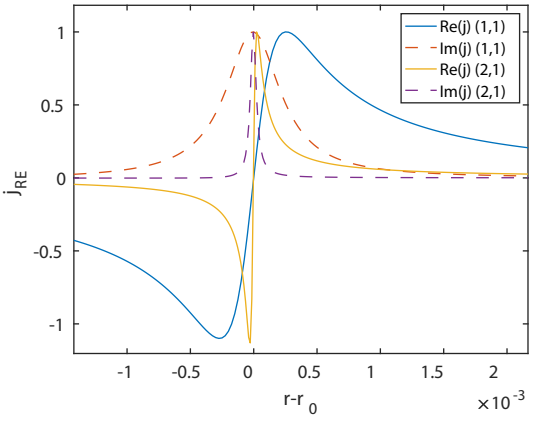

Figure 6. Runaway current structure of (1,1) resistive kink and (2,1) tearing mode with $c/v_A = 100$.

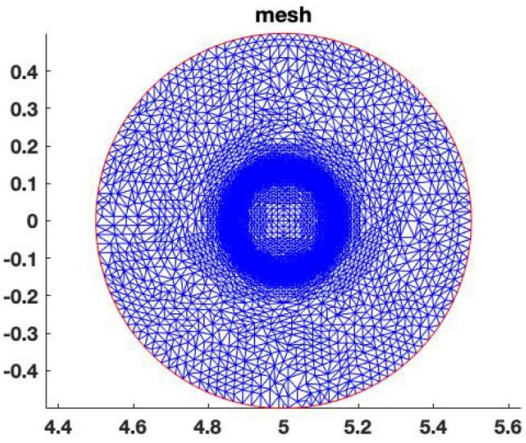

Figure 7. Mesh used for (1,1) resistive kink mode with runaway electrons case with M3D-C^1. Shown are the finite element mesh (blue) and the separatrix (red). The mesh has approximately 20000 elements.

4.1. $m = 1$, $n = 1$ resistive kink mode with runaway electrons

We have calculated the (1,1) mode described in section 3.1 using the same dimensionless parameters described there and in figure 1. We used the adaptive mesh illustrated in figure 7 where the typical size of the smallest triangles at the q = 1 surface was $d = 3 \times 10^{-4}a$. There is no equilibrium flow $\mathbf{V}_0$ and the initial electric field $\mathbf{E}_0$ is also zero. Here we also turned off the runaway source terms since we want to focus on the runaway-MHD interaction after the runaway current has saturated.

We illustrate the perturbed magnetic flux at 4 times in the M3D-C^1 calculation in figure 8. From analysis of the rotation, we see that it corresponds to a real part of the frequency of $\omega_r = 0.011 v_A/a$, in good agreement with the value $0.011 v_A/a$ found in section 3.1. Figure 9 and figure 10 show the perturbed runaway electron density and parallel current density for the (1,1) mode as calculated by M3D-C^1. The mode structure is

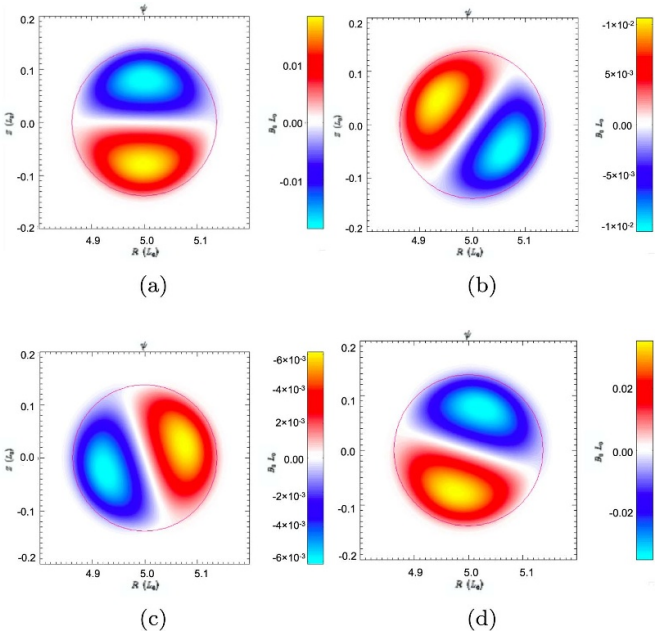

Figure 8. Time evolution poloidal of magnetic perturbation *psi* structure with (*a*) $t = 500\tau_A$, (*b*) $t = 1000\tau_A$, (*c*) $t = 1500\tau_A$, (*d*) $t = 2000\tau_A$.

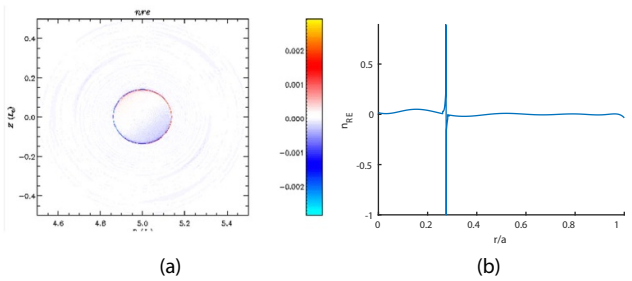

Figure 9. (*a*) Poloidal structure of runaway electron density perturbation and (*b*) (1,1) Fourier component of runaway density of (1,1) resistive kink mode with runaways.

peaked near the q = 1 rational surface which is shown in figure 10. The runaway current structure is also consistent with the results shown in figures 2(*b*) and (*c*). We have also performed the simulations using the same profiles without runaways and the result is in agreement with previous studies [9] in that there is no rotation.

We illustrate the time-step convergence properties of the M3D-C^1 computed growth rate in figure 11. It is seen that the converged growth rate in the limit of $\Delta t = 0$ is about $0.03\,545 v_A/a$, while the numerical eigenvalue solution is about $0.035\,2 v_A/a$ as shown in figure 11, only about a 1% deviation from the M3D-C^1 result. The growth rate and real frequency are converged when the element size is smaller than $1 \times 10^{-3} a$. We used a minimum mesh size of $3 \times 10^{-4} a$ to clearly see the radial structure of the runaway current.

We show in figure 12 the growth rate of the (1,1) mode as a function of resistivity for both the $I_{re}/I_0 = 0$ (no runaways in equilibrium) and $I_{re}/I_0 = 1$ (100% runaway current in equilibrium) cases for both the M3D-C^1 and eigenvalue calculations.

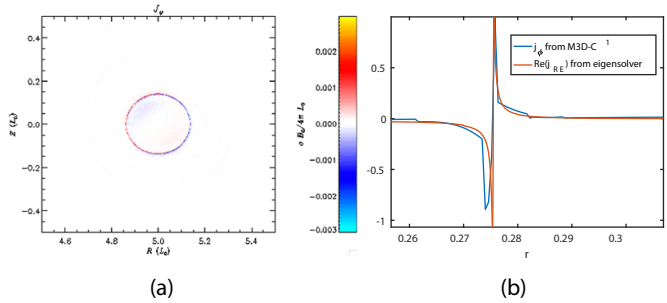

Figure 10. (*a*) Poloidal structure of parallel current perturbation and (*b*) (1,1) Fourier component of runaway current density of (1,1) resistive kink mode with runaways.

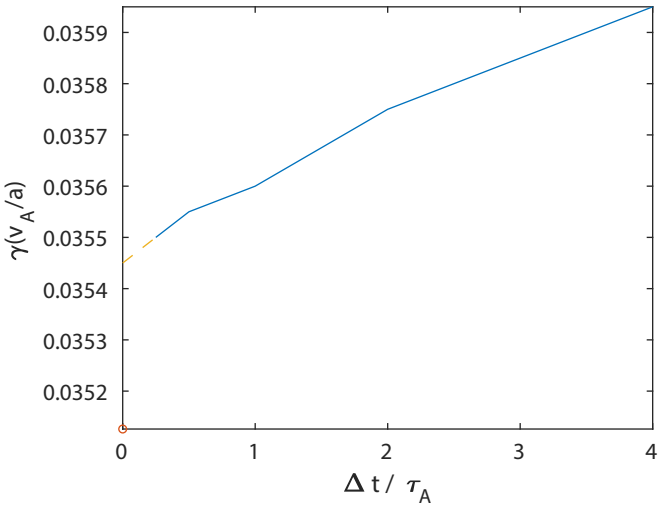

Figure 11. Time-step convergence of m = 1, n = 1, mode (solid line) and the numerical solution of the eigenfunction (circle).

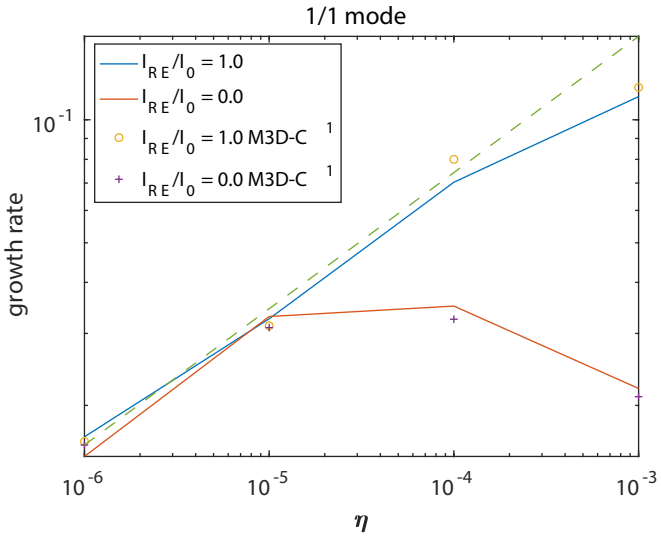

Figure 12. (1,1) resistive kink mode with runaway electrons eigenvalues and M3D-C^1 simulation with different resistivitiy, the dashed line is the 1/3 scaling law of the resistive mode, the solid lines are the results from numerical eigenvalue calculation and the dots and circles are the results from M3D-C^1 simulation.

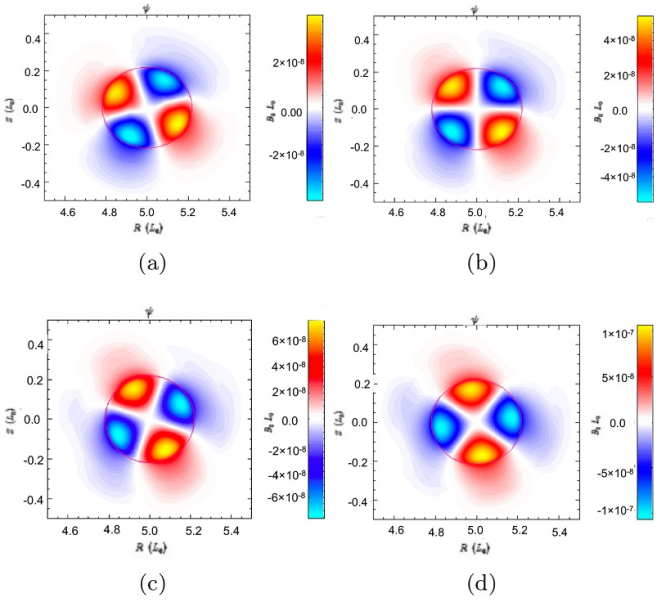

Figure 13. Poloidal magnetic flux *psi* structure time evolution with $t = 100\tau_A$ (*a*), $t = 150\tau_A$ (*b*), $t = 200\tau_A$ (*c*), $t = 250\tau_A$ (*d*).

For the case with no equilibrium runaways, both codes show the expected $\eta^{1/3}$ asymptotic scaling at small η but a turnover at larger η, so that γ decreases with increasing η [16]. For the cases with 100% of the current being carried by the runaways, the small η results are similar, but the large η turnover is much less pronounced.

4.2. *m = 2, n = 1 tearing mode with runaway electrons*

For the (2,1) tearing mode, we used a runaway speed of $c/v_A = 20$ and the same safety factor profile as shown in figure 4. The other input parameters are the same as for the (1,1) resistive kink in section 4.1.

The perturbed magnetic potential for the (2,1) mode from the M3D-C^1 calculation is shown in figure 13 at 4 times. From analyzing these, we conclude the real frequency was $|\omega_r| = 0.01 v_A/a$ compared to 0.008 8 for the eigenvalue code. There is also no rotation without runaways in the M3D-C^1 simulation. For this calculation, the mesh was refined about the q = 2 surface similar to what was done for the (1,1) mode at the q = 1 surface, but using higher resolution with $d = 2 \times 10^{-4} a$. The runaway density and current density are shown in figure 14 and figure 15. The runaway current is peaked near the q = 2 rational surface as shown in figure 15. In figure 15 we can see that the structure of the M3D-C^1 result is consistent with that calculated by the eigen-solver when the latter is run with $c/v_A = 20$. We also performed a similar time step convergence study for the (2,1) tearing mode with runaways. The growth rate extrapolated to $\Delta t = 0$ is about $0.006\,5 v_A/a$ and the numerical eigenvalue solution is about $0.00\,627 v_A/a$, which gives a deviation of about 4%. The growth rate and real frequency are also converged when the element size is smaller than $1 \times 10^{-3} a$. We used a minimum mesh size of $2 \times 10^{-4} a$ to clearly see the radial structure of the runaway current.

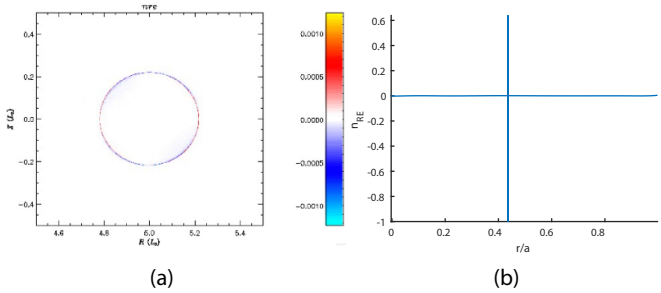

Figure 14. (*a*) Poloidal structure of runaway electron density perturbation and (*b*) normalized radial structure of the m = 2, n = 1 mode with runaway electron.

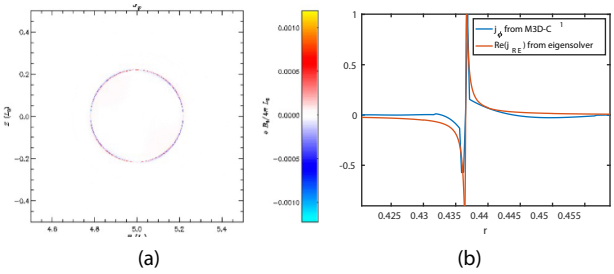

Figure 15. (*a*) Poloidal structure of parallel current density and (*b*) normalized radial structure of the m = 2, n = 1 mode with runaway electron.

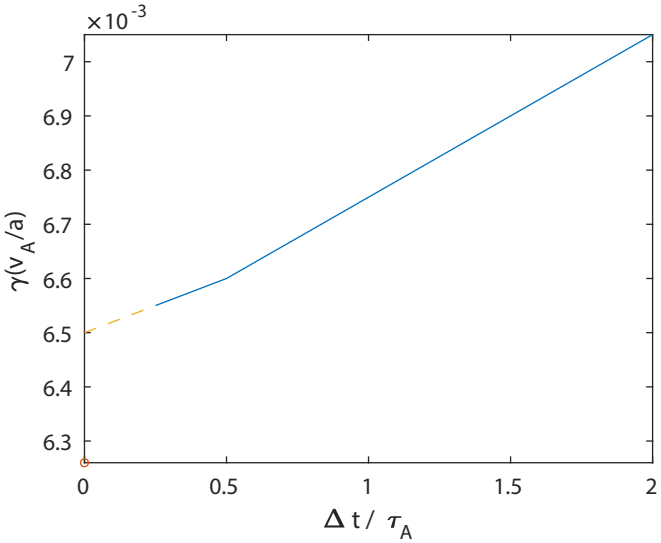

Figure 16. Time-step convergence of m = 2, n = 1, mode(solid line) and the numerical solution of the eigenfunction(circle).

We also show in figure 17 the growth rate of the (2,1) mode as a function of resistivity for both the $I_{re}/I_0 = 0$ (no runaways in equilibrium) and $I_{re}/I_0 = 1$ (100% runaway current in equilibrium) cases for both the M3D-C^1 and the eigen-solver. The trend is similar to that of figure 12 for the (1,1) mode.

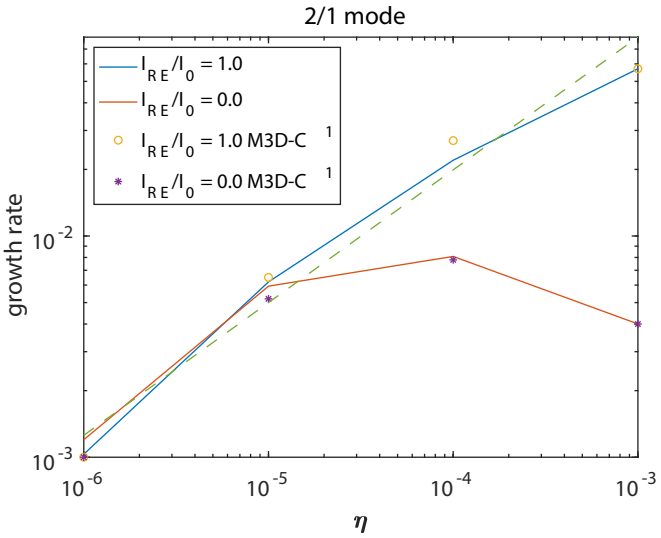

Figure 17. (2,1) tearing mode with runaway electrons eigenvalues and M3D-C^1 simulation with different resistivitiy, the dashed line is the 3/5 scaling low of the tearing mode, the solid lines are the results from numerical eigenvalue calculation and the dots and circles are the results from M3D-C^1 simulation.

5. Summary and discussion

We have implemented a runaway electron fluid model in the 3D, fully non-linear, finte beta MHD code M3D-C^1. The code now has the ability to calculate MHD instabilities including runaway electron current. In this paper, we have shown that it yields the correct results in the limit of a low-beta, linear, cylindrical plasma. The linear results of the (1,1) resistive kink and (2,1) tearing mode with runaway electrons have been verified against a numerical eigenvalue solution.

We also find that the runaway electron current can affect low mode number tearing mode toroidal current structure. The unstable mode is considerably more peaked around the rational surface when runaways are present. We also find that the radial scale length of toroidal current decreases as the runaway speed increases, consistent with previous studies [12].

The growth rate of the unstable mode is largely unaffected by the presence of runaways in the limit of small resistivity, $\eta \to 0$. However, at larger resistivities, the growth rate with runaways can be considerably larger than that without. The runaway current also causes a real frequency (rotation) and imaginary magnetic flux and current component to the (1,1) and (2,1) mode which has not previously been observed. It is a wave propagating in the plasma with a finite omega and a non-zero m and n number so that its volume integral vanishes. The electromagnetic wave propagation is mainly caused by the non-uniformity of the runaway current, which induces a phase velocity difference near the peaked runaway current perturbation and disappears when the initial runaway distribution is uniform. The magnitude of both the growth rate and real frequency are largely unchanged as the runaway velocity c changes from $10 < c/v_A < 200$, even as the perturbed current density becomes much more localized. Other benchmarks will be performed in the future as opportunities present themselves.

Acknowledgment

This work is supported by US DOE grant DE-AC02-09CH11466 and the SciDAC SCREAM and CTTS centers.

References

[1] Connor J.W. and Hastie R.J. 1975 *Nucl. Fusion* **15** 415
[2] Rosenbluth M.N. and Putvinski S.V. 1997 *Nucl. Fusion* **37** 1355
[3] Liu C., Hirvijoki E., Fu G.Y. 2018 *et al Phys. Rev. Lett.* **120** 265001
[4] Jardin s., Ferraro N. and Chen J., Breslau J.J. 2012 *Comput. Sci Discovery* **6** 014002
[5] Ferraro N.M. *et al* 2019 *Nucl. Fusion* **59** 016001
[6] Ferraro N.M. *et al* 2016 *Phys Plasmas* **23** 056114
[7] Zhang F. *et al* 2016 *Eng. Comput.* **32** 285–93
[8] Cai H. and Fu G. 2015 *Nucl. Fusion* **55** 022001
[9] Matsuyama A., Aiba N. and Yagi M. 2017 *Nucl. Fusion* **57** 066038
[10] Bandaru V. *et al* 2019 *Phys. Rev. E* **99** 063317
[11] Jardin 2010 *Computational Methods in Plasma Physics* (Boca Raton, FL: CRC Press)
[12] Helander P. *et al* 2007 *Phys. Plasmas* **14** 122102
[13] White R. 2001 *The Theory of Toroidally Confined Plasmas* 2nd ed (London: Imperial College Press)
[14] Coppi B. *et al* 1976 *Sov. J. Plasma Phys.* **2** 533
[15] Caramana E.J. 2004 *Comput. Phys.* **96** 484–93
[16] DeLucia J., Jardin S. and Glasser A. 1984 *Phys. Fluids* **27** 1470–82